Journal of Power Sources 182 (2008) 540–545

Contents lists available at ScienceDirect

Journal of Power Sources

journal homepage: www.elsevier.com/locate/jpowsour

Stress field and failure probability analysis for the single cell of planar solid oxide fuel cells

Tao Zhang[a,b], Qingshan Zhu[a,*], Wen Lai Huang[a], Zhaohui Xie[a], Xianshuang Xin[a]

[a] State Key Laboratory of Multi-Phase Complex Systems, Institute of Process Engineering, Chinese Academy of Sciences, Beijing 100190, People's Republic of China
[b] Graduate University of Chinese Academy of Sciences, Beijing 100049, People's Republic of China

ARTICLE INFO

Article history:
Received 3 March 2008
Received in revised form 11 April 2008
Accepted 11 April 2008
Available online 20 April 2008

Keywords:
Single cell
SOFC
Analytical model
Residual thermal stress
Failure probability

ABSTRACT

An analytical model is developed to predict the residual thermal stresses in a single cell of solid oxide fuel cells (SOFCs), which consists of a thick porous 8 mol% Y_2O_3 stabilized zirconia/nickel oxide (8YSZ/NiO) anode, a dense 8YSZ electrolyte and a porous lanthanum strontium manganite (LSM) cathode. The simulated stresses in the cell at room temperature, which are resulted from the contraction mismatch of its components, indicate that the major principal stress in the anode is tensile while the electrolyte and cathode are under compressive stresses. The stress in one component decreases with the increase of its thickness when the thicknesses of the other two components are fixed, and the decrease of the tensile stress in the anode will cause the increase of the compressive stresses in both the cathode and the electrolyte, and vice versa. The analysis also reveals that the anode is the part that is most susceptible to fracture since the tensile thermal stress is so high that it reaches to the fracture strength of the anode material. The Weibull statistic is employed to estimate the failure probability of the anode. The simulation results indicate that the anode failure probability decreases with the increase of the anode thickness and the decrease of the electrolyte thickness. To keep the anode failure probability less than 1E−06, the anode thickness should be greater than 0.7 mm for a cell with an electrolyte thickness of 10 μm and a cathode thickness of 20 μm.

1. Introduction

Solid oxide fuel cell (SOFC) is an electrochemical device, which directly converts the chemical energy into electricity with high efficiency and low pollutant emission. Though remarkable progress has been achieved in the development of SOFC in the recent years, the reliability of a planar SOFC remains a problem. The residual stresses, which arise mainly from the differences in the coefficients of thermal expansion (CTE) of the components, may destroy the structure of SOFC. When SOFC is cooled down to room temperature from an elevated temperature, the stresses in the cell reach to their maximum values and may lead to failure of the structure, i.e. delamination of the positive electrode–electrolyte–negative electrode (PEN), or formation of micro-cracks in the weak layers [1]. It was found that when the size of the planar cell was scaled up to an active area of much above 100 cm^2 they became prone to mechanical failure [2]. These experimental phenomena indicate that the reliability of SOFC is seriously dependent on the residual thermal stresses.

The residual stresses in SOFC have been investigated both experimentally and theoretically in literature. It has been demonstrated that the residual stresses in SOFC cell could be determined by the X-ray diffraction method [3–5]. The residual stresses were also theoretically analyzed using finite-element analysis (FEA) by several authors [5–8]. Since the options of materials are quite limited for the anode, electrolyte and cathode materials of the planar SOFC, the dimension becomes one of the main factors that may be used to reduce the residual thermal stresses in the PEN. Although finite-element analysis (FEA) has been performed to estimate the stress distribution in a PEN, the influence of the dimensions (e.g. the thickness of each layer) of PEN on the stress distributions has not yet been investigated in detail. In order to obtain some guidelines to reduce the stresses in the PEN to enhance its reliability, an analytical model was developed, and by which the influence of PEN dimensions on the stress field and failure probability was investigated in this study.

2. Analytical model

The analytical model in this study focused on the main stresses resulted from the differential thermal expansion coefficients of the

* Corresponding author at: State Key Laboratory of Multi-Phase Complex Systems, Institute of Process Engineering, Chinese Academy of Sciences, Zhong Guan Cun, Haidian District, P.O. Box 353, Beijing 100190, People's Republic of China.
Tel.: +86 10 62536108; fax: +86 10 62536108.
E-mail address: qszhu@home.ipe.ac.cn (Q. Zhu).

0378-7753/$ – see front matter.
doi:10.1016/j.jpowsour.2008.04.027

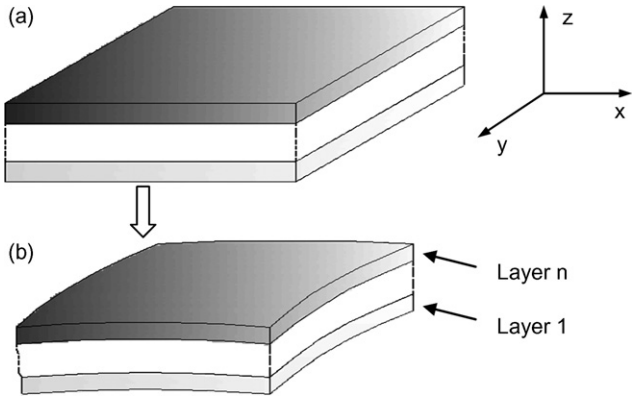

Fig. 1. Conceptual model for the generation of residual thermal stresses in a multilayer system: (a) stress-free condition and (b) bending and balance of bending moment.

components of a PEN during cooling from an elevated temperature to room temperature. In this model, the components bonded together in a SOFC cell were modeled as a flat multilayer plate.

In an elastic multilayer system, the origin of residual thermal stresses developed during the cooling is illustrated in Fig. 1. An elastic multilayer plate under stress-free condition at elevated temperatures is shown schematically in Fig. 1(a), where the thickness of ith layer is t_i. The subscript i denotes the layer number ranging from 1 to n, with 1 representing the layer at the bottom. The coordinate system is defined such that the free surface of the 1st layer is located at $z = 0$, and the interface between layers i and $i+1$ is located at $z = h_i$. With these definitions, the relation between h_i and t_i is described by Ref. [9]:

$$h_i = \sum_{j=1}^{i} t_j (1 \le i \le n,\ 1 \le j \le i) \tag{1}$$

The analysis is generally based on the classical beam bending theory. In the cooling process, the tensile or compressive stresses are imposed on all layers, to achieve displacement compatibility, while the total forces remain zero. Bending is allowed to occur to balance the bending moment induced by the asymmetric stresses in the previous step. Naturally, these processes occur simultaneously in the actual multilayer systems [10].

The force balance and bending moment balance equations can be expressed as

$$\sum F = \sum_{1}^{n} \int_{h_{i-1}}^{h_i} E_i^* \varepsilon_i \mathrm{d}z = 0 \tag{2}$$

$$\sum M = \sum_{1}^{n} \int_{h_{i-1}}^{h_i} E_i^* \varepsilon_i (z - \delta) \mathrm{d}z = 0 \tag{3}$$

where F and M are the force and bending moment, respectively, δ is the distance from the bending axis [9] to the free surface of the 1st layer ($z = 0$), E_i^* and ε_i are the effective Young's modulus value and strain of the ith layer, respectively.

In this system, an equal biaxial stress state ($\sigma_x = \sigma_y$), with the negligible stress through thickness ($\sigma_z = 0$), is assumed [11]. The σ_y stress will induce a strain in the x-direction, due to a Poisson effect. The net strain in the x-direction can thus be written as

$$\varepsilon_x E = \sigma_x - \nu(\sigma_y + \sigma_z) = \sigma_x(1 - \nu) \tag{4}$$

So that the relation between stress and strain in the x-direction can be expressed as

$$\frac{\sigma_x}{\varepsilon_x} = \frac{E}{1 - \nu} = E^* \tag{5}$$

This effective Young's modulus value, E^*, should be used in the above and following equations.

In analyzing thermal stresses in bilayer systems, Hsueh and Evans found that a general equation could be used to describe the strain distribution in the system [10]. This was achieved by decomposing the total strain, ε, into a stress strain, ε_s, and a bending strain, ε_b, and the relation between ε and ε_s, ε_b can be described as

$$\varepsilon = \varepsilon_s + \varepsilon_b \tag{6}$$

In this case, the strain continuity condition is automatically satisfied.

The coefficient of thermal expansion (CTE) of any layer is α_i, respectively. Considering the whole system cooled from a stress-free state, to a certain temperature, T, the stress strain in the ith layer, $\varepsilon_{s,i}$, produced during the cooling temperature range, ΔT, is given by

$$\varepsilon_{s,i} = \alpha_i \Delta T - \varepsilon_0 \tag{7}$$

where ε_0 is the linear shrinkage of the multilayer system without bending during the cooling temperature range.

The stress strain of the individual layer is generated due to the in-plane forces resulted from the mismatch of CTEs between one layer and the others, while the bending strain of the individual layer is generated due to the bending moment of the whole system. According to the elementary bending theory of flat plates, the bending strain can be expressed as [11]:

$$\varepsilon_b = K(z - \delta) \tag{8}$$

where K is the curvature.

In the case of pure bending, the bending stress above the bending axis is equal and opposite to those below in order for no net normal force to be presented, that is:

$$\sum_{i=1}^{n} \int_{h_i - t_i}^{h_i} K E_i^* (z - \delta) \mathrm{d}z = 0 \tag{9}$$

From Eqs. (2), (3) and (9), $\varepsilon_{s,i}$, δ and K can be obtained and expressed as

$$\varepsilon_{s,i} = \frac{\sum_{j=1}^{n} E_j^* t_j (\alpha_i - \alpha_j) \Delta T}{\sum_{j=1}^{n} E_j^* t_j} \tag{10}$$

$$\delta = \frac{\sum_{i=1}^{n} E_i^* t_i (2h_i - t_i)}{2\sum_{i=1}^{n} E_i^* t_i} \tag{11}$$

$$K = \frac{-3\sum_{i=1}^{n} E_i^* \varepsilon_{s,i} [2h_i t_i - t_i^2 - 2\delta t_i]}{2\sum_{i=1}^{n} E_i^* [(h_i - \delta)^3 - (h_i - t_i - \delta)^3]} \tag{12}$$

where the subscripts, i and j, denote the layer number.

As discussed above, in the ith layer, the strain is composed of two parts. With $\varepsilon_{s,i}$, K and δ, the total strain in the ith layer, ε_i, can be obtained. Substituting ε_i into Eq. (5), the residual thermal stress distributions that are related to z-axis in the ith layer can be obtained and expressed as

$$\sigma_i = E_i^* [\varepsilon_{s,i} + K(z - \delta)] \tag{13}$$

The calculation normally starts from a stress-free state at an elevated temperature to room temperature. Since the practical components of a single cell are sintered step by step, and the layers are bonded at different temperatures, it is assumed that the

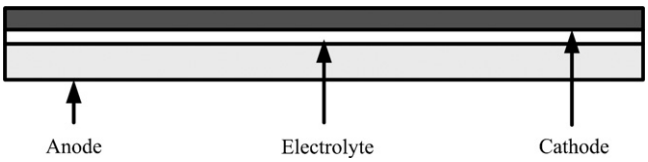

Fig. 2. Cross-section of a typical cell.

layer at or above its bonding temperature could deform plastically and the thermal stress in it is free. During the cooling, the further shrinkage will induce additional stresses in the compositive multilayer system. Therefore, the calculation is performed from the highest bonding temperature to the lowest bonding temperature and then room temperature. Finally, the strains set up in every step are summarized, thus the total stresses could be obtained from Eq. (13).

3. Results and discussion

The bending beam method based on the elastic properties, Poisson's ratio, and coefficients of thermal expansion of the materials has often been used to estimate the residual stresses in multilayer systems [9]. In this study, a typical multilayer single cell, whose cross-section is shown in Fig. 2, consisting of a thick porous anode of 8 mol% Y_2O_3 stabilized zirconia/nickel oxide (8YSZ/NiO), a dense 8YSZ electrolyte and a porous cathode of lanthanum strontium manganite (LSM), was modeled with the assumption that the residual stresses were only caused by the mismatch of CTEs. The mechanical properties needed for the stress calculation are listed in Table 1.

3.1. Stress fields in the half-cell

The stress fields in the half-cell consisting of a porous 8YSZ/NiO anode layer and a dense 8YSZ electrolyte layer were first calculated to validate the analytical model, as they had been experimentally measured before [3–5]. In the calculation, it was assumed that the stresses in the half-cell only started to build up below the lowest plastic deformation temperature and the temperature was assumed to be 1360 °C, as it had been reported that the 8YSZ/NiO–8YSZ half-cell could be flattened at 1360 °C to eliminate warp [5] due to plastically deformation.

The simulation residual thermal stresses in the electrolytes with various thicknesses of the electrolyte and the anode at room temperature are shown in Fig. 3. Note that the residual thermal stresses are independent of the in-plane location, as indicated by Eqs. (9)–(13). It shows that the stress is always compressive in the electrolyte layer due to the lower CTE of the electrolyte as compared with that of the anode layer, varying from 600 to 850 MPa dependent on the thicknesses of the anode and the electrolyte. As illustrated in Fig. 3, at a fixed anode thickness the stress decreases with the increase of the electrolyte thickness, while at a fixed electrolyte thickness the stress decreases with the decrease of the anode thickness.

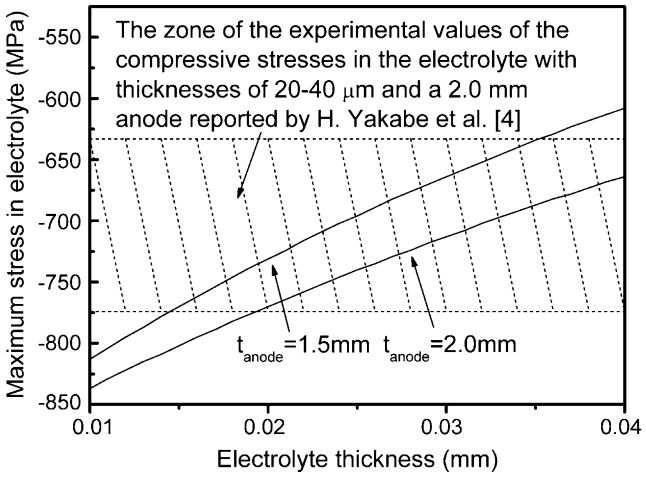

Fig. 3. Simulation residual thermal stresses in the electrolytes with various thicknesses of the electrolyte and the anode at room temperature.

In order to check whether the calculated stresses were reasonable, experimental data determined by Yakabe et al. [3,4] and Fischer et al. [5] were employed to compare with the calculated results. Yakabe et al. reported that the compressive stresses varied from 633 to 774 MPa with 20–40 μm electrolyte layers on anodes of 2.0 mm. The experimentally measured stresses are in very good agreement with our calculated results. The change trend of the stress is also consistent with the results disclosed by this analytical model. Fischer et al. [5] reported a compressive thermal stress of 560 ± 35 MPa for a half-cell with an anode thickness of 1.5 mm and an electrolyte thickness of 10 μm. The thermal stress in Fischer's case is lower but still within the same order of magnitude as compared with those of Yakabe's data and our simulation results. This is possibly due to the different specimen conditions, for example, the difference in anode composition, anode density, and electrolyte density will influence the Young's modulus of these materials and the thermal stresses. It is noted that it is difficult to make direct comparison between experimental data and simulation results, as the information of exact geometrical and material properties is not available for the stresses reported. From these comparisons, it is clear that the thermal stresses could be well predicted by the analytical model.

3.2. Stress fields in the cell

In the present simulation, the half-cell and the cathode are assumed to be sintered together at 1250 °C to form an assembly [3], and at this temperature the thermal stress in the cathode is assumed to be free. The maximal stresses in the three layers are shown in Fig. 4, noting that negative denotes compressive stress while positive means tensile stress. Here the effect of the thickness of each layer on the residual stresses in the PEN will be especially studied.

From Fig. 4, several distinct features can be easily identified. Firstly, the stress in the anode is always tensile (at the interface

Table 1
Material properties of the components in the PEN

Materials	Young's modulus (GPa)	Poisson's coefficient	Coefficient of thermal expansion ($\times 10^{-6}$ K^{-1})	Fracture strength (MPa)
Cathode (LSM)	35 [12]	0.25 [12]	11.7 [13]	52 [14]
Electrolyte (8YSZ)	212 [15]	0.32 [14]	10.8 [13]	1000[a] [16]
Anode (NiO–8YSZ)	55 [17]	0.17 [17]	13.0[b]	50–100 [5]

[a] Compressive fracture strength of 8YSZ.
[b] Measured with a dilatometer (L75/1550, Linseis Messgeraete GmbH, Germany) in the temperature range of 20–1360 °C, the sample is the same as that in Ref. [18].

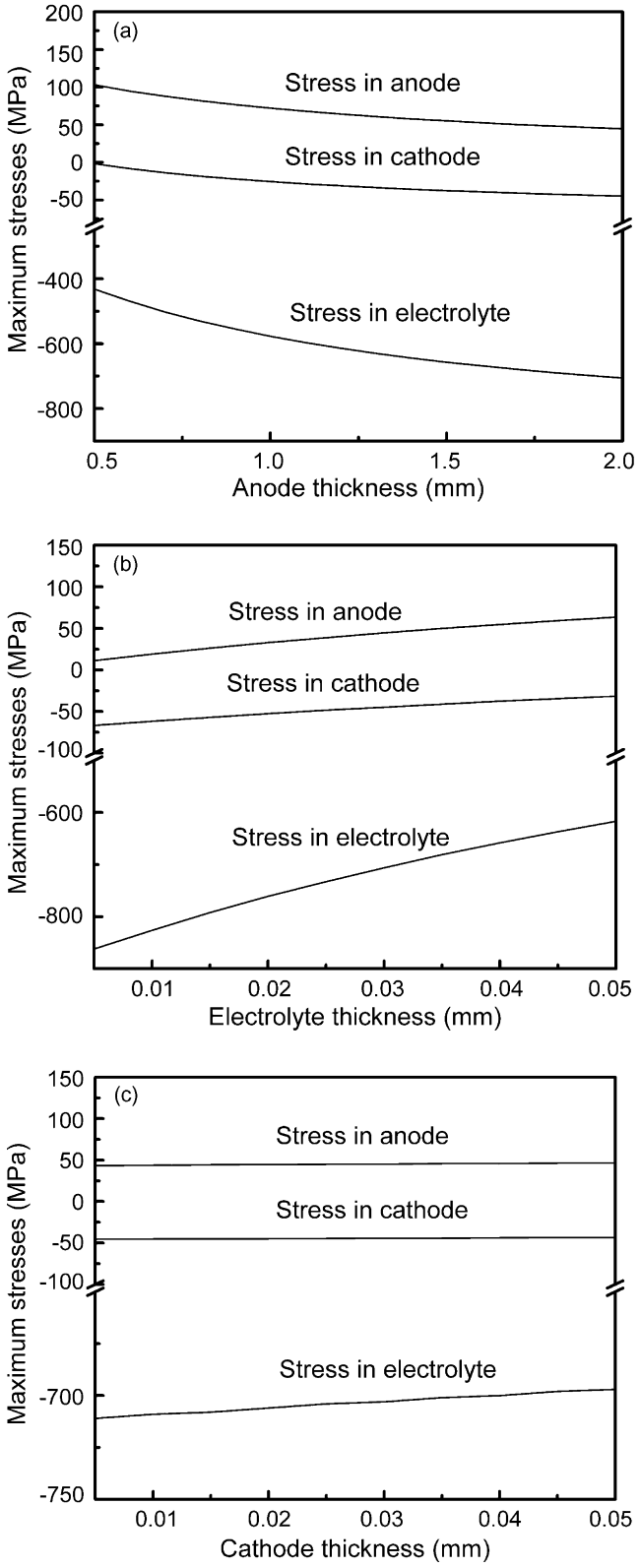

Fig. 4. Maximum stresses in the PENs with various thicknesses: (a) $t_{electrolyte}$ = 0.03 mm, $t_{cathode}$ = 0.02 mm; (b) t_{anode} = 2.0 mm, $t_{cathode}$ = 0.02 mm; and (c) t_{anode} = 2.0 mm, $t_{electrolyte}$ = 0.03 mm.

between the anode and the electrolyte, the stress at the free surface is compressive, which is not shown in Fig. 4, and the value of the maximum compressive stress is less than that of the maximum tensile stress), while the stresses in the cathode and the electrolyte are compressive, primarily due to the lower CTE of the cathode and the electrolyte materials. Secondly, the stress in one component decreases with the increase of its thickness, when the thicknesses of the other two components are fixed. In addition, the decrease of the tensile stress in the anode will cause the increase of the compressive stresses in both the cathode and the electrolyte, and vice versa. Thirdly, the thicknesses of the anode and the electrolyte have pronounced influence on the thermal stresses in the PEN, while the influence of the cathode thickness on the stresses is marginal. Finally, the magnitudes of stresses are quite different for the different layers. The stresses in the anode and the cathode are normally less than 100 MPa, while the stress in the electrolyte can exceed 800 MPa.

It is well known that ceramic materials are susceptible to fracture under tensile stress, while being less susceptible to fracture under compressive stress. Therefore, the compressive fracture strength of a ceramic material is normally much greater than its tensile fracture strength. The above analysis indicates that the cathode is unlike to crack since the cathode only experiences a low level of compressive stress. The compressive stress in the 8YSZ electrolyte is much higher, reaching 500–800 MPa, but still below the critical level as the compressive fracture strength of 8YSZ has been reported to be greater than 1 GPa [16]. However, the stress becomes critical for the anode as the tensile thermal stress in the anode is in the range of 45–95 MPa, which is in the same order of magnitude as compared with the fracture strength (e.g. 50–100 MPa) of the NiO–8YSZ anode [5]. This analysis suggests that the anode is the layer that is most susceptible to fracture in the PEN. Therefore, the stress in the anode should be first optimized in order to improve the reliability of the PEN.

3.3. Failure probability analysis and optimization of the thicknesses

The failure of a SOFC stack is often caused by the fracture of the PEN due to the brittle nature of the ceramic materials. From the previous section, it is clear that the anode is the part that is most susceptible to fracture in the PEN. It is therefore valuable to analyze the failure probability of the anode for the purpose of the reliability improvement of the PEN.

The failure probability of brittle materials like ceramics is often modeled by Weibull statistics as

$$P = 1 - \exp\left[-\left(\frac{\sigma}{\sigma_0}\right)^m\right] \tag{14}$$

where σ_0 and m are the characteristic strength and the Weibull parameter, respectively. With this model, one could calculate the failure stress σ at a given probability P. Assuming that the failure of the PEN is solely caused by the thermal stress accumulated during cooling from a stress-free state at elevated temperatures to room temperature, a criterion that describes the failure probability of the PEN may be formulated as

$$\sigma_{thermal,a} = E_a^*[\varepsilon_{s,a} + K(t_a - \delta)] \le \sigma_a = \sigma_0 \exp\left(-\frac{1}{m}\ln(1-P)\right) \tag{15}$$

where the subscript, a, denotes the anode.

This non-linear multivariate equation correlates the failure probability with the geometric parameters, which are concealed in ε, K and δ, of the PEN.

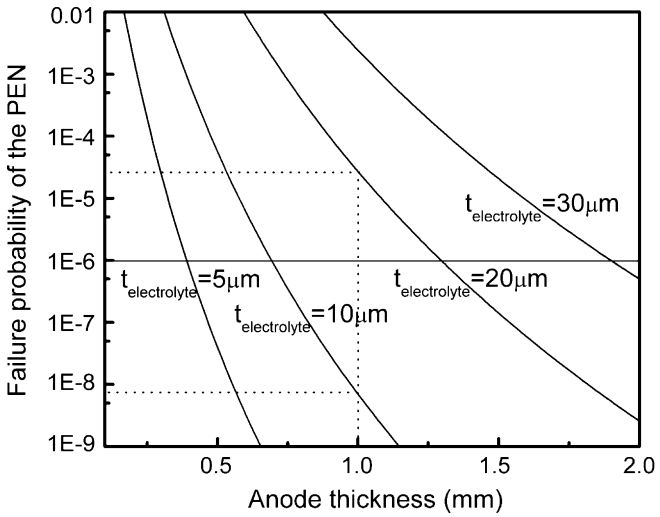

Fig. 5. Failure probability of the PEN with various thicknesses of the anode and the electrolyte.

With Eq. (15), the minimum anode thickness could be determined by numerical method at given conditions like the electrolyte thickness, the cathode thickness and the allowed failure probability together with predetermined model parameters of σ_0 and m. The σ_0 and m of the "standard anode", e.g. density and 8YSZ/NiO ratio close to the real anode used for SOFC, without the electrolyte and cathode layers, were determined by Y. Wang et al. [19] to be 91.24 and 16.7 MPa, respectively. These values were consequently employed in the present study.

Since the influence of the cathode thickness on the thermal stresses was marginal, the thickness of the cathode was fixed to 20 μm for easy presenting the influence of the anode and the electrolyte thicknesses on the failure probability of the PEN. For practical applications, it was pointed out that the failure probability of SOFCs should be less than 1E−05 [20] or even less than 1E−06 [20,21]. In this study, the failure probability of the PEN was set to 1E−06.

With the above-mentioned parameters and assumptions, the influence of the thicknesses of the anode and the electrolyte on the failure probability of the PEN is shown in Fig. 5. It shows that at a given electrolyte thickness the failure probability decreases with increasing anode thickness, while the failure probability increases with increasing electrolyte thickness at a fixed anode thickness. This figure also reveals that the electrolyte thickness has pronounced influence over the failure probability of the PEN. The failure probability shows nearly four orders of magnitude increase, from 9E−09 to 3E−05, when the electrolyte thickness increases from 10 to 20 μm with the anode thickness of 1.0 mm. From the figure, one could also determine the minimum anode thickness at a fixed electrolyte thickness and a given failure probability. For anode-supported SOFC, thin electrolytes are normally favorable for reducing the resistance of the electrolyte, and the electrolyte thickness employed in literature [5,22] is in the range of 10–20 μm in most cases. It could thus be calculated that the anode thickness should be at least in the range of 0.7–1.3 mm for such electrolytes in order to keep the failure probability less than 1E−06.

The thicknesses of the anode, the electrolyte and the cathode may be varied within certain ranges without significant influence on the electrochemical properties of the PEN. In literature the electrolyte thickness is usually in the range of 5–30 μm [3–5], the anode thickness is normally in the range of 0.7–2.0 mm [3–6,23]. These acceptable variation ranges would provide enough space for optimizing the dimensions of the PEN. Since a small change in the electrolyte/anode thickness would have significant influence over the failure probability of the PEN, it is highly possible that the failure probability of the anode and the PEN could be greatly reduced through manipulating the thicknesses of the anode and the electrolyte within the ranges. Therefore, the model could be quite useful for the PEN dimensions design to improve the reliability of the PEN.

4. Conclusions

An analytical model based on the classical beam bending theory for predicting the residual thermal stresses in SOFC single cell was developed in this study. The model was concerned with the residual stresses in the single cell only arising from the contraction mismatch of its components, but other practical factors, such as mechanical support structure, rigid seals, etc., which could also affect the stress fields in the cell when it was assembled in a SOFC stack, were not considered here. The model was validated by experimental data. Simulations reveal that the stress in the anode is tensile in the range of 45–95 MPa, while the electrolyte and cathode are under favorable compressive stresses in the range of 500–800 and 20–60 MPa, respectively. The stress in one component decreases with the increase of its thickness when the thicknesses of the other two components are fixed. Calculations also show that the anode is the part that is most susceptible to fracture due to the tensile thermal stress close to the fracture strength of the anode material.

The Weibull statistic was incorporated to the model for investigating the influence of cell dimensions on the failure probability of the anode. The anode failure probability decreases with the increase of the anode thickness and the decrease of the electrolyte thickness. Moreover, a small change in the electrolyte/anode thickness will have significant influence over the failure probability of the PEN. The increase of the electrolyte thickness from 10 to 20 μm will cause nearly four orders of magnitude increase of the anode failure probability. Consequently, there exists a minimum anode thickness at given conditions like the electrolyte/cathode thickness, failure probability, etc. The model can be used to design and optimize the PEN dimensions.

Acknowledgement

This work has been financially supported by the National Natural Science Foundation of China (Grant No. 50730002).

References

[1] A. Selcuk, G. Merere, A. Atkinson, J. Mater. Sci. 36 (2001) 1173–1182.
[2] Structural Limitations in the Scale-up of Anode Supported SOFCs, Final report to DOE NETL, TIAX, LLC, October 2002.
[3] H. Yakabe, Y. Baba, T. Sakurai, M. Satoh, I. Hirosawa, Y. Yoda, J. Power Sources 131 (2004) 278–284.
[4] H. Yakabe, Y. Baba, T. Sakurai, Y. Yoshitaka, J. Power Sources 135 (2004) 9–16.
[5] W. Fischer, J. Malzbender, G. Blass, R.W. Steinbrech, J. Power Sources 150 (2005) 73–77.
[6] C.-K. Lin, T.-T. Chen, Y.-P. Chyou, L.-K. Chiang, J. Power Sources 164 (2007) 238–251.
[7] A. Selimovic, M. Kemm, T. Torisson, M. Assadi, J. Power Sources 145 (2005) 463–469.
[8] H. Yakabe, T. Ogiwara, M. Hishinuma, I. Yasuda, J. Power Sources 102 (2001) 144–154.
[9] C.H. Hsueh, Thin Solid Films 418 (2002) 182–188.
[10] C.H. Hsueh, A.G. Evans, J. Am. Ceram. Soc. 68 (1985) 241–248.
[11] Y.C. Tsui, T.W. Clyne, Thin Solid Films 306 (1997) 23–33.
[12] N.M. Sammes, Y. Du, The mechanical properties of ceramic materials for solid oxide fuel cells, Electrochem. Proc. 97 (18) (2000) 671–679.
[13] N.Q. Minh, T. Takahashi, Science and Technology of Ceramic Fuel Cells, Elsevier, 1995.
[14] A. Atkinson, A. Selcuk, Solid State Ionics 134 (2000) 59–66.
[15] M. Radovic, E. Lara-Curzio, Acta Mater. 52 (2004) 5747–5756.

[16] T. Kato, N.S. Wang, A. Negishi, A. Momma, Y. Kasuga, K. Nozaki, Proceedings of the Third International Fuel Cell Conference, Nagoya, November 3, 1999, p. 461.
[17] C.H. Hsueh, C.R. Luttrell, P.F. Becher, Int. J. Solids Struct. 43 (2006) 6014–6025.
[18] W.L. Huang, Q. Zhu, Z. Xie, J. Power Sources 162 (2006) 464–468.
[19] Y. Wang, M.E. Walter, K. Sabolsky, M.M. Seabaugh, Solid State Ionics 177 (2006) 1517–1527.
[20] C.S. Montross, H. Yokokawa, M. Dokiya, Br. Ceram. Trans. 101 (2002) 85–93.
[21] A. Nakajo, C. Stiller, G. Harkegard, O. Bolland, J. Power Sources 158 (2006) 287–294.
[22] F.L. Lowrie, R.D. Rawlings, J. Eur. Ceram. Soc. 20 (2000) 751–760.
[23] V.A.C. Haanappel, J. Mertens, J. Malzbender, J. Power Sources 171 (2007) 789–792.